Monthly Notices of the ROYAL ASTRONOMICAL SOCIETY

MNRAS **540,** L48–L53 (2025) https://doi.org/10.1093/mnrasl/slaf031
Advance Access publication 2025 April 7

Doppler shifted transient sodium detection by KECK/HIRES

Athira Unni [1,2★] Apurva V. Oza [3,4] H. Jens Hoeijmakers,[5] Julia V. Seidel,[6] Thirupathi Sivarani,[2] Carl A. Schmidt,[7] Aurora Y. Kesseli,[8] Katherine de Kleer,[3] Ashley D. Baker,[9] Andrea Gebek,[10] Moritz Meyer zu Westram,[11] Chloe Fisher [12] Steph Sallum,[1] Manjunath Bestha[2] and Aaron Bello-Arufe[4]

[1]*Department of Astronomy and Astrophysics, University of California, Santa Cruz, CA 95064, USA*
[2]*Indian Institute of Astrophysics, Bangalore 560034, India*
[3]*Division of Geological and Planetary Sciences, California Institute of Technology, Pasadena, CA 91125, USA*
[4]*Jet Propulsion Laboratory, California Institute of Technology, Pasadena, CA 91011, USA*
[5]*Department of Astronomy and Theoretical Physics, Lund University, Box 118, 221 00 Lund, Sweden*
[6]*European Southern Observatory, Alonso de Córdova 3107, Vitacura, Región Metropolitana, Chile*
[7]*Center for Space Physics, Boston University, 685 Commonwealth Ave, Boston, MA 0221, USA*
[8]*Caltech/IPAC-NASA Exoplanet Science Institute , Pasadena, CA 91125, USA*
[9]*Department of Astronomy, California Institute of Technology, Pasadena, CA 91125, USA*
[10]*Sterrenkundig Observatorium, Universiteit Gent, Krijgslaan 281, S9, B-9000 Gent, Belgium*
[11]*Astronomical Institute, University of Bern, Sidlerstrasse 5, 3012 Bern, Switzerland*
[12]*Department of Physics, University of Oxford, Parks Rd, Oxford OX1 3PU, UK*

Accepted 2025 April 2. Received 2025 April 1; in original form 2024 July 28

ABSTRACT

We carried out the first high-resolution transit observations of the exoplanet WASP-49 Ab with Keck/HIRES. Upon custom wavelength calibration we achieve a Doppler RV precision of < 60 m s^{-1}. This is an improvement in RV stability of roughly 240 m s^{-1} with respect to the instrument standard. We report an average sodium flux residual of $\Delta\mathcal{F}_{\rm NaD}/\mathcal{F}_{\star}(\lambda) \sim 3.2 \pm 0.4$ per cent (8.0σ) comparable to previous studies. Interestingly, an average Doppler shift of -6.2 ± 0.5 km s^{-1} ($12.4\,\sigma$) is identified offset from the exoplanet rest frame. The velocity residuals *in time* trace a blueshift ($v_{\Gamma,\rm ingress} \sim -10.3 \pm 1.9$ km s^{-1}) to redshift ($v_{\Gamma,\rm egress} \sim +4.1 \pm 1.5$ km s^{-1}) suggesting the origin of the observed sodium is unlikely from the atmosphere of the planet. The average Na light curves indicate a depth of $\Delta\mathcal{F}_{\rm NaD}/\mathcal{F}_{\star}(t) \sim 0.47 \pm 0.04$ per cent ($11.7\,\sigma$) enduring $\lesssim 90$ min with a half-max duration of ~ 40.1 min. Frequent high-resolution spectroscopic observations will be able to characterize the periodicity of the observed Doppler shifts. Considering the origin of the transient sodium gas is of unknown geometry, a co-orbiting natural satellite may be a likely source.

Key words: techniques: spectroscopic – exoplanets – planets and satellites: atmospheres – planets and satellites: composition – planets and satellites: gaseous planets.

1 INTRODUCTION

High-Resolution Transmission Spectroscopy (HRTS) is a powerful tool for exoplanet atmospheric characterization. High spectral resolution allows us to resolve and detect individual atomic and molecular species without the help of atmospheric retrieval models (Snellen et al. 2008). It is also possible to detect signatures of global circulation and contamination from stellar chromospheric emission. The first high-resolution exoplanet transit spectra were successfully obtained for HD189733b (Redfield et al. 2008) using the High-Resolution Spectrograph at the Hobby–Eberly Telescope. Apart from this, VLT/ESPRESSO (Pepe et al. 2013), HARPS-N/GIANO (Cosentino et al. 2012; Claudi et al. 2017) at the Telescopio Nazionale Galileo (TNG), CARMENES (Quirrenbach et al. 2010) at Calar Alto Observatory, and SPIRou (McLean, Ramsay & Takami 2012) at the Canada France Hawaii Telescope (CFHT) showed their capability of HRTS observations. Sodium is considered to be a commonly studied element in the optical part of the transmission spectra of hot Jupiters and hot Saturns (Redfield et al. 2008; Snellen et al. 2008; Wood et al. 2011; Zhou & Bayliss 2012; Burton et al. 2015; Wyttenbach et al. 2015, 2017; Jensen et al. 2018; Allart et al. 2020; Chen et al. 2020; Seidel et al. 2020a, b; Ishizuka et al. 2021; Kawauchi et al. 2022). Due to the large resonance scattering cross-section, sodium allows for detections at high altitudes where the annulus of gas is expected to be rarefied and tenuous, in the planet's alkali exosphere (Gebek & Oza 2020).

Here we carefully study the NaD line region of WASP-49 Ab during the transit using the high-resolution transit observation from Keck/HIRES. WASP-49 Ab orbits a G6V star ($V_{\rm mag} = 11.35$, distance = 194.5 pc) with a transit duration of 2.14 h and a mass of $0.37 M_J$ (Lendl et al. 2012). The first, high-resolution transmission spectra of WASP-49 Ab were obtained using HARPS/3.6-m spec-

★ E-mail: athira.exo@gmail.com

trograph by Wyttenbach et al. (2017), revealing anomalous sodium of $\mathrm{d}F_{\mathrm{Na}}/F_{\star}(\lambda) \approx 1.99$ per cent and 1.83 per cent for D_2 and D_1 lines, respectively. The observed neutral sodium was reported to be extended up to $\sim$ 1.5 times the planetary radii to reproduce the observed sodium transit depth. This is roughly three times the Na I altitude probed at any known exoplanetary system to date (Langeveld, Madhusudhan & Cabot 2022; Sicilia et al. 2025).

Suppose we assume the origin of this sodium is endogenic, or from the atmosphere of the planet itself, then a supersolar sodium abundance or a super-heated atmospheric layer at WASP-49b may be plausible in reproducing the average altitude probed of neutral sodium. However, when atmospheric escape due to incoming irradiation is studied, the upper atmosphere cools and the line depth observed by HARPS/3.6-m could not be reproduced (Cubillos et al. 2017). Meanwhile, sodium in non-local thermodynamic equilibrium (N-LTE) was also suggested as a source (Fisher & Heng 2019). In the case of an exogenic sodium, the possible sources can be an older cometary impact or a natural satellite orbiting around the planet WASP-49 A b (Oza et al. 2019).

Here we present the first Keck/HIRES observation of WASP-49b to understand the sodium anomaly. The paper is outlined as follows. In Section 2, we summarize the observations and the data reduction. A detailed wavelength re-calibration and analysis are presented in Section 3. Followed by the discussion and the results are presented in Section 4. Finally, Section 5 presents the conclusion.

2 OBSERVATION AND DATA REDUCTION

HIgh Resolution Echelle Spectrograph (HIRES) is designed to be a general-purpose spectrograph installed on the Nasmyth platform of the Keck-I telescope. A wavelength range of 3000–10000 Å for the spectrograph is achieved using two different cross-dispersers and collimators. Three separate CCDs cover the entire echelle order of the spectra with an average spectral resolution of $\mathcal{R} = 67\,000$ (Vogt et al. 1994).

One complete transit of WASP-49 Ab was observed with HIRES on 2019 November 11 (Programme ID: C284). The observation started from UT 10:28:41 (hh:mm:ss) to 16:15:05 with an exoplanet mid-transit time at 13.31 UT (Julian Date 2458799.06791922). A total of 42 exposures of 420 s each covered ingress, egress, complete transit, and out-of-transit phases. The sky was clear throughout the night. The typical SNR of the observation was 55 (at mid-transit). The airmass and the seeing varied from 1.30 to 1.76 and 0.6 to 1.2 arcsec, respectively from the beginning to the end of the observation. We used the MAKEE pipeline reduced data from the Keck Observatory Archive (KOA) for the analysis. The continuum normalization of each order of all the spectra was performed using IRAF with a cubic spline fitting.

3 CUSTOM WAVELENGTH CALIBRATION

The first successful attempt at using Keck/HIRES for the exoplanet atmospheric sodium detection was by Langland-Shula et al. (2009) for the exoplanet HD 209 458 b. As they were focused on detecting the broad-band, low-resolution sodium feature from the atmosphere of HD 209 458 b rather than constructing high-resolution transit spectra, a linear shift using a cross-correlation in the wavelength solution was sufficient. HIRES is not housed inside a thermal or pressure-controlled environment; hence it is expected that there could be instrument drift that will cause a shift in the wavelength dispersion solution during the observations. Though slit spectrographs provide high throughput, the line spread function (LSF) can vary significantly

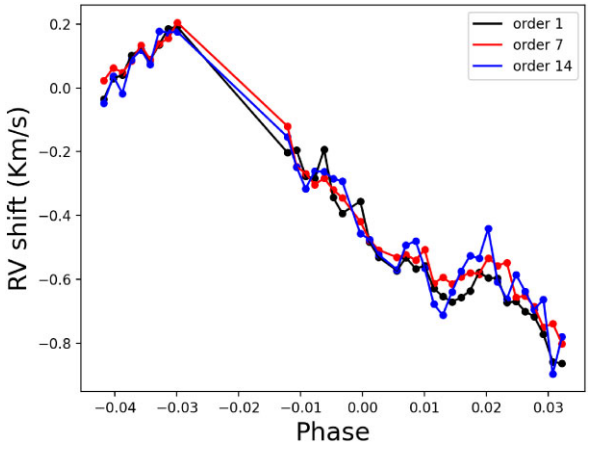

Figure 1. The velocity shift in each exposure with respect to the reference exposure as a function of phase is shown for three echelle orders (HIRES CCD2). The first order is in black, the last order is in blue, and the order containing the sodium doublet around 5890 Å is in red. There is a shift of 0.8 Km s^{-1} during the complete observation period.

during the observations. Due to this, the wavelength position on the detector shifts, and the wavelength dispersion solution could also change. The stability of the wavelength dispersion solution is crucial to perform HRTS observations.

To achieve the maximum wavelength precision, we used the first out-of-transit spectra as a reference and shifted all the exposures with respect to the reference exposure. Fig. 1 shows the velocity shift across the exposures over the complete observation period, which is about 0.8 km s^{-1}. We corrected this shift for individual exposures, which is significant for accurate telluric subtraction and detecting the residual transit velocity signal from the planet.

3.1 Distortion correction

The residual wavelength drift after correcting the linear velocity shift (Fig. 1) could arise due to optical distortion caused by aberration and varying anamorphism at the detector. And it is found to be $\pm$ 300 m s^{-1}. Ideally, re-deriving the wavelength dispersion solution will remove the error due to residual wavelength distortion. However, the ThAr calibration exposures were not taken during transit to maximize the transit coverage. So we used the stellar lines themselves to correct for the residual wavelength distortion errors separately for individual orders. For this purpose, we selected all the possible clean stellar lines from each order and found the wavelength centroid of these absorption lines using a Gaussian fit (Fig. 2). The shift in the centroid wavelength of each selected line, relative to the corresponding absorption line in the first exposure is estimated. These residual shift is not constant across the order and the magnitude of the residual distortion in wavelength was found to scale with overall instrument drift and minimum at the centre of each order and increase as we go down to both edges of each order as shown in Fig. 3. A cubic spline was then fitted to these measured wavelength shifts in each order, relative to the reference measurements from the first exposure. Best-fitting cubic spline coefficients in each order are used for wavelength re-calibration. Finally, we achieve a velocity precision of $\leq$ 60 m s^{-1} (Fig. A1 in Appendix) for the sodium doublet order. This is the minimum shift that can be achieved using 1D extracted spectra from Keck/HIRES. However, the first exposure itself can have a significant distortion. Therefore, we cross-correlate each exposure with respect

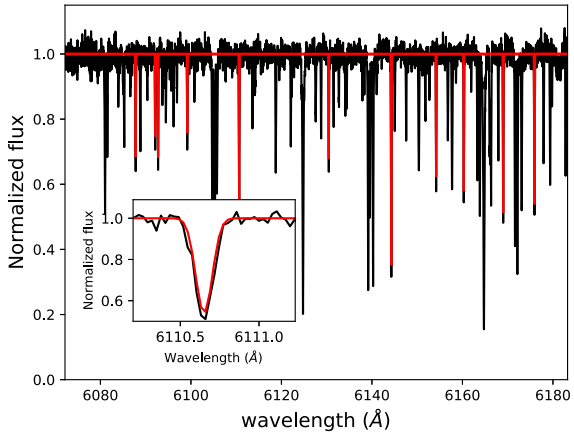

Figure 2. Observed spectra (in black) and selected clean stellar lines (red) for calculating the residual distortion. A Gaussian fit to the lines is shown in red. A zoomed version of a Gaussian fit is shown in the subplot.

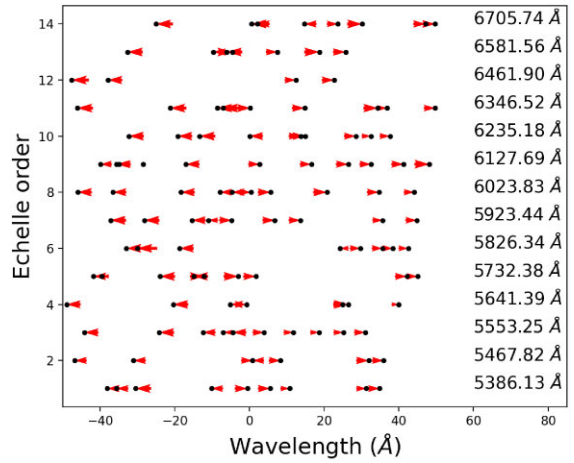

Figure 3. A residual RV shift vector map across different echelle orders is shown here. The possible residual shift in each exposure is calculated by measuring the centroid of a set of lines in each exposure (Fig. 2). The calculated shift in each line (0.0001 times length of the red arrow) with respect to the centroid of the corresponding line in the first exposure (black dot). The centre wavelength of each order is considered to be zero. The y-axis represents the order number in Keck/HIRES CCD2. Also, the centre wavelength of each order is mentioned on the right side of the plot.

to the synthetic solar spectra of the same spectral resolution, bringing all exposures to Stellar Rest Frame (C.f. Fig. A2).

4 RESULTS

We followed the steps outlined in Seidel et al. (2019) to obtain the final transmission spectrum. Telluric correction was performed on the normalized spectra using *molecfit* (Kausch et al. 2015; Smette et al. 2015), version 1.5.1. *Molecfit* is a well-established tool, successfully used over the years by, e.g. Allart et al. (2017), Hoeijmakers et al. (2020), Seidel et al. (2020a, b), Kawauchi et al. (2022), and Stangret et al. (2022). All telluric corrected spectra in the Stellar Rest Frame (SRF) are separated into exposures taken during transit and out-of-transit, based on the transit ingress ($\phi_{\rm exoplanet} = -0.016$) and egress phases ($\phi_{\rm exoplanet} = 0.016$). Finally, we obtained 17 exposures taken during the transit and 20 spectra taken outside the transit event, after removing a couple of exposures with lower SNR.

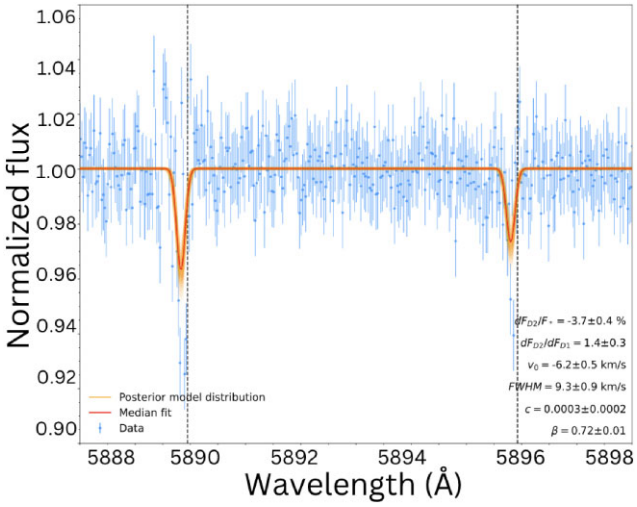

Figure 4. Final transmission spectrum from Keck/HIRES best-fitting Gaussian model along with the raw data. The average amplitude of the best-fitting Gaussian is $dF_{\rm Na}/F_* = 3.2\pm0.4$ per cent (8.0–σ), FWHM $= 9.3 \pm 0.9$ km s^{-1} and continuum c. Uncertainties are scaled with β as a free-fitting parameter. The residual sodium signal is blueshifted at $v_0 = -6.2 \pm 0.4$ km s^{-1}.

The residual spectra are obtained by dividing each in-transit spectra by the master out-of-transit spectra. These residuals are then shifted back to the Planet Rest Frame (PRF) by applying the estimated orbital velocity of the planet at each exposure. We use values consistent with Oza et al. (2024): orbital period 2.78174 d, semimajor amplitude 0.0378 AU, inclination 84.48 degrees, and the RV semi-amplitude of 151.468 km s^{-1} (Wyttenbach et al. 2017). The final transmission spectra in the sodium doublet region are shown in Fig. 4. To model the sodium doublet and its associated error, we assumed both lines are Gaussian, with peak absorption depth ($\Delta\mathcal{F}_{\rm NaD}/\mathcal{F}_\star$), centroid velocity ($v_0$) and FWHM ($\sigma$), along with a flat continuum at c as free parameters. A prior σ value of 2.0 km s^{-1} used for the model convergence. We achieve a 8.0–σ detection of neutral sodium corresponding to an average NaD transit depth of $\Delta\mathcal{F}_{\rm NaD}/\mathcal{F}_\star = 3.2 \pm 0.4$ per cent with a D_2/D_1 ratio of 1.4. Interestingly, the residual signal shows an overall blueshift of -6.2 ± 0.5 km s^{-1} along with a 12.4–σ detection. The posterior distribution of the best-fitting model is shown in Fig. 5.

As the host star WASP-49 A is a slow rotator and less active star ($\log R_{HK} = -5.17$; Cegla et al. 2016), the chances of stellar contamination of the observed sodium is very unlikely. Wyttenbach et al. (2017) did a detailed study to understand the Rossiter–McLaughlin effect (RM) and found no significant impact of the RM effect on the transmission spectra at sub km s^{-1} levels. The centre-to-limb variations in the sodium D lines are also not significant in the case of G-type stars like WASP-49 A (Czesla et al. 2015; Khalafinejad et al. 2017; Wyttenbach et al. 2017). Due to the relatively high systemic velocity (41.73 km s^{-1}), the stellar sodium lines are well separated from the interstellar medium lines. The ratio of the D_2/D_1 lines is generally indicative of the optical depth of the atmospheric or exospheric medium (Gebek & Oza 2020). The Keck/HIRES data supports a more tenuous sodium exosphere $f_{D_2/D_1} \sim 1.4 \pm 0.3$, suggesting the sodium may indeed be at the border of an optically thin/optically thick medium ($\tau_\nu \sim 0.7 - 3$). Fig. 6 shows the residual sodium spectra for the D_2 line as a function of radial velocity at different orbital phases during transit. Flat spectra before and after transit (black) confirm the insignificant stellar contamination.

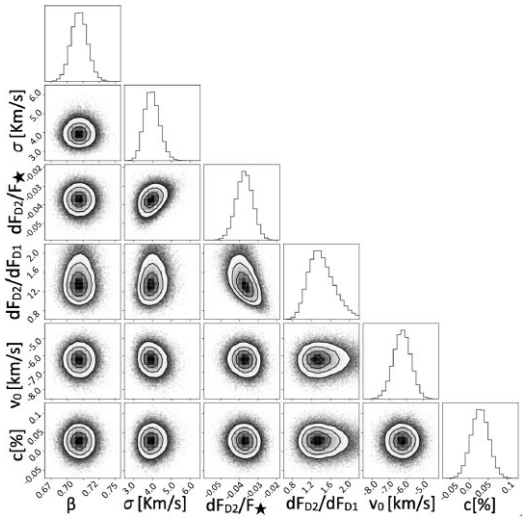

Figure 5. Posterior distributions of the model parameters describing the Na doublet as a pair of Gaussian where the average D_2 and D_1 line depth is reported $dF_{\rm Na}/F_*$, centroid velocity shift v_0, width σ, sodium D_2 to D_1 line ratio dF_{D2}/dF_{D1}, and continuum c. The uncertainties are scaled with β which is a free fitting parameter.

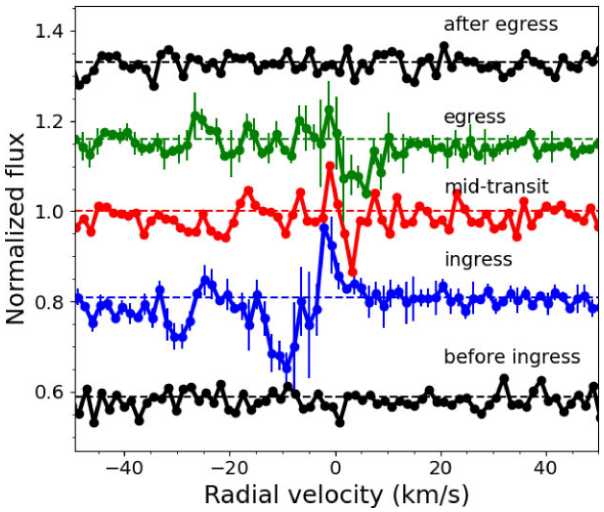

Figure 6. Doppler shifts versus exoplanet phase for the NaD_2 line. Blue indicates ingress, red indicates mid-transit, and green indicates the egress part of the transit. Evidently, the largest residual peak is indeed blueshifted as described in the text. At egress, there is a significant redshift (Fig. A3 shows the stacked residual spectra for all the exposures). A constant y-offset is applied for visibility purposes. We note that the Rossiter–Mclaughlin effect cannot generate signals larger than 100 ppm (Wyttenbach et al. 2017).

A blue-to-red shift can be seen as we move from ingress (blue) to egress (green) of the transient feature. We combine three exposures centred at $\phi_{\rm exoplanet} = -0.0076$ referred to as ingress, three exposures centred at $\phi_{\rm exoplanet} = -0.0018$ exoplanet mid-transit, and three exposures centred at $\phi_{\rm exoplanet} = +0.0076$ referred to as egress of the transient sodium feature. The observed Na I Doppler shifts are distributed blueward, with an average shift of -6.2 ± 0.5 km s^{-1} of the planetary rest frame, even though the residual at egress is surprisingly redshifted at $\sim +4.1 \pm 1.5$ km s^{-1} and the ingress is blueshifted at roughly -10.3 ± 1.9 km s^{-1}. We confirm variable Doppler behaviour at high-significance with $> 5\sigma$ blueshifts, and

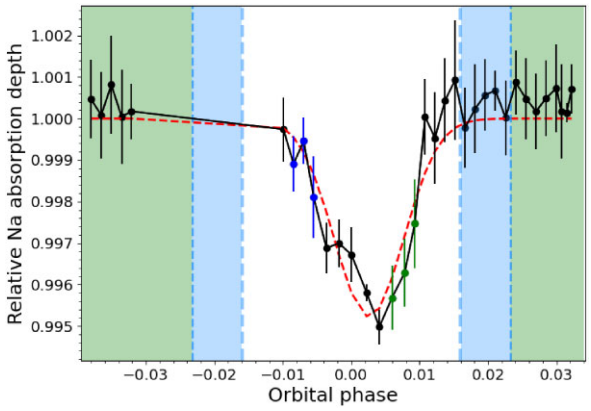

Figure 7. Average neutral sodium light curve constructed using 1.5 Å band width from the core of both Na D_1 and Na D_2 lines. The white region indicates the transit duration, the blue region is $\sim \frac{1}{2}$ the Hill sphere, and the green region indicates the out-of-transit observation. The estimated transit duration of the sodium signal from the best-fitting Gaussian (red dashed line) is 40.05 ± 3.2 min. The average value of the blue and green data points used as ingress and egress in Fig. 6, respectively.

$\sim 3\sigma$ redshifts, reported at $+9.7 \pm 1.6$ km s^{-1} in HARPS/3.6-m Epoch II data (Oza et al. 2024).

To confirm the origin, we further analysed the sodium signature as a function of time (Seidel et al. 2019; Oza et al. 2024). We constructed a narrow band light curve by averaging sodium D lines of 1.5 Å width centred around each line. Fig. 7 shows the average sodium transit light curve of WASP-49b at $d\mathcal{F}/\mathcal{F}(t) \sim 0.47$ per cent $\pm$ 0.04 per cent(11.7σ). Compared to the 129-min exoplanet transit window, we find a Gaussian FWHM duration of $\Delta t_{\rm NaD} \sim 40.05$ min (average residual duration over >3-sigma), roughly 90 min shorter than the exoplanet transit duration. Interestingly, the duration of the transient sodium in the light curve is also reported to be roughly $\sim$ 40 min by Oza et al. (2024), which we confirm here at 11.7 σ. The velocity asymmetry shown in Fig. 6 is different from kinematic behaviour usually observed in other hot Jupiters (Ehrenreich et al. 2020; Kesseli et al. 2022). For a hot Jupiter, generally a redshift or no velocity shift is measured at ingress followed by a blueshift at egress, which is expected if the signal is coming from a planet rotating synchronously in the direction of its orbit. A signal that is more blueshifted at ingress could indicate the observed sodium is not from the atmospheric limb of the planet. The magnitude of the velocity shift is also similar to an ultra-hot ($T_{\rm eq} \gtrsim 2000$ K) planetary jet escaping from an exoplanet atmosphere (Seidel et al. 2023), where the kinetic temperatures probed at 1 nanobar has been reported to exceed $\sim$ 12 000 K (Huang et al. 2023). Multi-epoch sodium light-curve observations thus far of this hot Saturn indicate the observed sodium is Doppler-shifted and transient, which we confirm here, likely associated with the orbit of a natural satellite (Oza et al. 2024). Recent dynamical studies demonstrate low-eccentricity exomoons are indeed stable at orbits in between 1.2 and 1.5 R_p (Sucerquia & Cuello 2025). Dozens of more large-aperture, precise high-resolution transmission spectroscopy observations are needed to build up a radial velocity follow up of the Doppler shift presented here. High-cadence infrared observations of volcanic gases (SO_2, CO_2) or grains (SiO_2) would be especially useful in tandem with high-resolution optical observations.

5 CONCLUSION

In summary, we observed one complete transit of the hot Saturn WASP-49 b, including significant stellar baseline using Keck/HIRES. Using a custom wavelength calibration technique, we were able to achieve a wavelength precision of 60 m s^{-1}. This work demonstrates the feasibility of using slit-based spectrographs Keck/HIRES for high-resolution exoplanet transit spectroscopy. Here, we identify an average residual sodium flux of $d\mathcal{F}_{\rm Na}/\mathcal{F}_{\star}(\lambda) = 3.2 \pm 0.4$ per cent in transmission spectra (8.0 σ), with an observed Doppler shift of -6.2 ± 0.5 km s^{-1} suggests the neutral sodium gas is moving with respect to the exoplanet. The approximate flux of the transient feature in the transmission light curve is: $d\mathcal{F}_{\rm Na}/\mathcal{F}_{\star}(t) = 0.47 \pm 0.04$ per cent which is smaller than the HARPS/3.6-m (Oza et al. 2024). The kinematic Na I results indicate that the source of the observed sodium is unlikely from the atmosphere of the planet, yet from a natural satellite orbiting around the planet, although we cannot be sure of its orbit or the geometry of its clouds based on this transit alone.

ACKNOWLEDGEMENTS

We acknowledge the Keck telescope facility and archive facility for providing the observation time and reduced data. We would like to acknowledge the Exo-Io team for all the support and help. The research described in this paper was carried out in part at the Jet Propulsion Laboratory, California Institute of Technology, under a contract with the National Aeronautics Space Administration ©2025. All rights reserved. Some of the data presented herein were obtained at Keck Observatory, which is operated as a scientific partnership among the California Institute of Technology, the University of California, and the National Aeronautics and Space Administration. The Observatory was made possible by the generous financial support of the William. M. Keck Foundation. The authors wish to recognize and acknowledge the very significant cultural role and reverence that the summit of Maunakea has always had within the Native Hawaiian community. We are most fortunate to have the opportunity to conduct observations from this mountain.

DATA AVAILABILITY

The observed Keck/HIRES data is available on the Keck Observatory Archive (KOA). The wavelength recalibrated data will be provided by the corresponding author upon reasonable request.

REFERENCES

Allart R., Lovis C., Pino L., Wyttenbach A., Ehrenreich D., Pepe F., 2017, A&A, 606, A144
Allart R. et al., 2020, A&A, 644, A155
Burton J. R., Watson C. A., Rodríguez-Gil P., Skillen I., Littlefair S. P., Dhillon S., Pollacco D., 2015, MNRAS, 446, 1071
Cegla H. M., Lovis C., Bourrier V., Beeck B., Watson C. A., Pepe F., 2016, A&A, 588, A127
Chen G., Casasayas-Barris N., Pallé E., Yan F., Stangret M., Cegla H. M., Allart R., Lovis C., 2020, A&A, 635, A171
Claudi R. et al., 2017, Eur. Phys. J. Plus, 132, 1
Cosentino R. et al., 2012, in McLean I. S., Ramsay S. K., Takami H., eds, Proc. SPIE Conf. Ser. Vol. 8446, Ground-based and Airborne Instrumentation for Astronomy IV. SPIE, Bellingham, p. 657
Cubillos P. E. et al., 2017, ApJ, 849, 145
Czesla S., Klocová T., Khalafinejad S., Wolter U., Schmitt J. H. M. M., 2015, A&A, 582, A51
Ehrenreich D. et al., 2020, Nature, 580, 597
Fisher C., Heng K., 2019, ApJ, 881, 25
Gebek A., Oza A. V., 2020, MNRAS, 497, 5271
Hoeijmakers H. J. et al., 2020, A&A, 641, A123
Huang C., Koskinen T., Lavvas P., Fossati L., 2023, ApJ, 951, 123
Ishizuka M., Kawahara H., Nugroho S. K., Kawashima Y., Hirano T., Tamura M., 2021, AJ, 161, 153
Jensen A. G., Cauley P. W., Redfield S., Cochran W. D., Endl M., 2018, AJ, 156, 154
Kausch W. et al., 2015, A&A, 576, A78
Kawauchi K., Narita N., Sato B., Kawashima Y., 2022, PASJ, 74, 225
Kesseli A. Y., Snellen I. A. G., Casasayas-Barris N., Mollière P., Sánchez-López A., 2022, AJ, 163, 107
Khalafinejad S. et al., 2017, A&A, 598, A131
Langeveld A. B., Madhusudhan N., Cabot S. H. C., 2022, MNRAS, 514, 5192
Langland-Shula L. E., Vogt S. S., Charbonneau D., Butler P., Marcy G., 2009, ApJ, 696, 1355
Lendl M. et al., 2012, A&A, 544, A72
McLean I. S., Ramsay S. K., Takami H., 2012, in McLean I. S., Ramsay S. K., Takami H., eds, Proc. SPIE Conf. Ser. Vol. 8446, Ground-based and Airborne Instrumentation for Astronomy IV. SPIE, Bellingham, p. 844601
Oza A. V. et al., 2019, ApJ, 885, 168
Oza A. V. et al., 2024, ApJ, 973, L53
Pepe F. et al., 2013, The Messenger, 153, 6
Quirrenbach A. et al., 2010, in McLean I. S., Ramsay S. K., Takami H., eds, Proc. SPIE Conf. Ser. Vol. 7735, Ground-based and Airborne Instrumentation for Astronomy III. SPIE, Bellingham, p. 455
Redfield S., Endl M., Cochran W. D., Koesterke L., 2008, ApJ, 673, L87
Seidel J. V. et al., 2019, A&A, 623, A166
Seidel J. V. et al., 2020a, A&A, 641, L7
Seidel J. V. et al., 2020b, A&A, 643, A45
Seidel J. V. et al., 2023, A&A, 673, A125
Sicilia D. et al., 2025, A&A, 693, A316
Smette A. et al., 2015, A&A, 576, A77
Snellen I. A. G., Albrecht S., de Mooij E. J. W., Le Poole R. S., 2008, A&A, 487, 357
Stangret M., Casasayas-Barris N., Pallé E., Orell-Miquel J., Morello G., Luque R., Nowak G., Yan F., 2022, A&A, 662, A101
Sucerquia M., Cuello N., 2025, A&A, 694, L8
Vogt S. S. et al., 1994, in Crawford D. L., Craine E. R., eds, Proc. SPIE Conf. Ser. Vol. 2198, Instrumentation in Astronomy VIII. SPIE, Bellingham, p. 362
Wood P. L., Maxted P. F. L., Smalley B., Iro N., 2011, MNRAS, 412, 2376
Wyttenbach A., Ehrenreich D., Lovis C., Udry S., Pepe F., 2015, A&A, 577, A62
Wyttenbach A. et al., 2017, A&A, 602, A36
Zhou G., Bayliss D. D. R., 2012, MNRAS, 426, 2483

APPENDIX A

This paper has been typeset from a TEX/LATEX file prepared by the author.

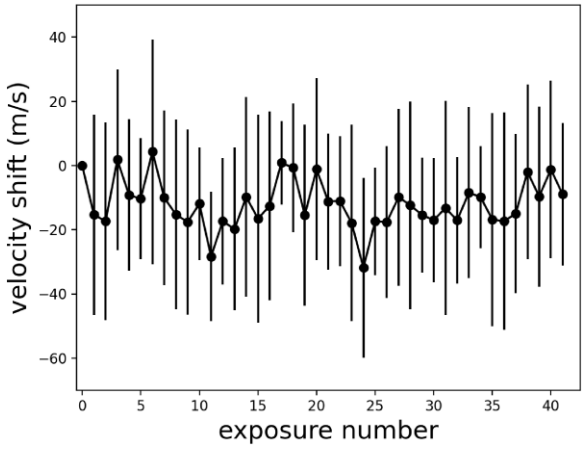

Figure A1. The velocity precision of the wavelength solution achieved by Keck/HIRES after distortion correction for the echelle order with sodium. Each data point is the average wavelength shift in all the clean absorption line in an exposure.

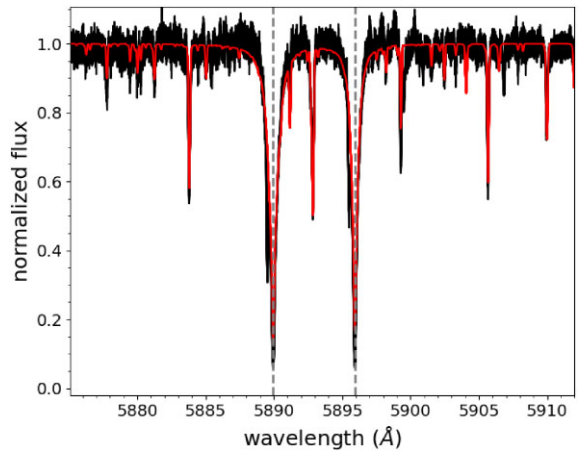

Figure A2. All the HIRES exposures (black) overplotted with the Phoenix model in the Stellar Rest Frame. The vertical dashed lines (grey) show the position of Na D lines in the Stellar Rest Frame.

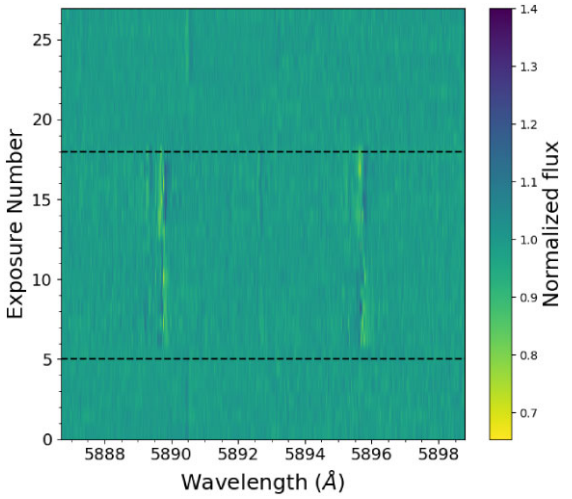

Figure A3. Doppler-shifted sodium detection in the Stellar Rest Frame (SRF). The region within the horizontal lines shows the exoplanet transit event. The colourbar indicates the normalized flux.